



1 **A Study of Earthquake Recurrence based on a One-body**
2 **Spring-slider Model in the Presence of Thermal-pressurized**
3 **Slip-weakening Friction and Viscosity**

4

5 Jeen-Hwa Wang

6 Institute of Earth Sciences, Academia Sinica, P.O. Box 1-55, Nangang, Taipei,

7 TAIWAN (e-mail: jhwang@earth.sinica.edu.tw)

8

9

10

11 **Abstract** Earthquake recurrence is studied from the temporal variation in slip
12 through numerical simulations based on the normalized form of equation of motion of
13 a one-body spring-slider model with thermal-pressurized slip-weakening friction and
14 viscosity. The main parameters are the normalized characteristic displacement, U_c , of
15 the friction law and the normalized damping coefficient (to represent viscosity), η .
16 Define T_R , D , and τ_D to be the recurrence time of events, the final slip of an event,
17 and the duration time of an event, respectively. Simulation results show that T_R
18 increases when U_c decreases or η increases; D and τ_D decrease with increasing η ; and
19 τ_D increases with U_c . The time- and slip-predictable model can describe the temporal
20 variation in cumulative slip. When the wear process is taken into account, the
21 thickness of slip zone, h which depends on the cumulated slip, $S(t)=\sum D(t)$, i.e.,
22 $h(t)=CS(t)$ (C =a dimensionless constant) is an important parameter on T_R and D . U_c is
23 a function of h and thus depends on C . In the computational time period, the wear
24 process influences the recurrence of events and such an effect increases with C when



25 $C > 0.0001$. Both T_R and D decrease when the fault becomes more mature, thus
26 suggesting that it is more difficult to produce large earthquakes along a fault when it
27 becomes more mature. Neither the time-predictable model nor the slip-predictable one
28 can describe the temporal variation in $S(t)$ under the wear process with large C .

29

30 **Key Words:** Recurrence of events, final slip, rise time, one-body spring-slider
31 model, thermal-pressurized slip-weakening friction, characteristic displacement,
32 viscosity, wear process

33

34

35 **1 Introduction**

36 Earthquake recurrence that is relevant to the physics of faulting is an important
37 factor in seismic hazard assessment. It is related to the seismic cycle, which represents
38 the occurrence of several earthquakes in the same segment of a fault during a time
39 period. Fig. 1 exhibits the general pattern of time variation in slip during a seismic
40 cycle. In the figure, T_R is the recurrence (also denoted by repeat or inter-event) time
41 of two events in a seismic cycle, τ_D is the duration time of slip of an event, and D is
42 the final slip of an event. Sykes and Quittmeyer (1981) pointed out that the major
43 factors in controlling T_R are the plate moving speed and the geometry of the rupture
44 zone. Based on Reid's elastic rebound theory (Reid, 1910), Schwartz and
45 Coppersmith (1984) assumed that an earthquake occurs when the tectonic shear stress
46 on a fault is higher than a critical level, which is dependent on the physical conditions
47 of the fault and the loading by regional tectonics. Since in their work a fault has a
48 homogeneous distribution of physical properties under constant tectonic loading,
49 earthquakes could happen regularly.



50 Some observations exhibit periodicity for different size earthquakes. Bakun and
51 McEvelly (1979) obtained $T_R \approx 23 \pm 9$ years for $M \approx 6$ earthquakes at the Parkfield
52 segment of the San Andreas fault, USA since 1857. Sykes and Menke (2006)
53 estimated $T_R \approx 100$ years for $M \geq 8$ earthquakes in the Nankaido trough, Japan. Okada et
54 al. (2003) gained $T_R = 5.5 \pm 0.7$ years for earthquakes with $M = 4.8 \pm 0.1$ off Kamaishi,
55 Japan, since 1957. Nadeau and Johnson (1998) inferred an empirical relation between
56 T_R and seismic moment, M_o : $T_R \propto M_o^{1/6}$. To make this relation valid, the stress drop,
57 $\Delta\sigma$, or the long-term slip velocity of a fault, v_l , must be in terms of M_o . Based on
58 three data set from eastern Taiwan, Parkfield, USA, and northeastern Japan, Chen et
59 al. (2007) inferred $T_R \sim M_o^{0.61}$. Beeler et al. (2001) proposed a theoretical relation:
60 $T_R = \Delta\sigma^{2/3} M_o^{1/3} / 1.81 \mu v_l$, where μ is the rigidity of the fault-zone materials, under
61 constant $\Delta\sigma$ and v_l .

62 However, the main factors in influencing earthquake occurrences commonly are
63 spatially heterogeneous and also vary with time. Thus, the recurrence times of
64 earthquakes, especially large events, are not constant inferred either from observations
65 (Ando, 1975; Sieh, 1981; Kanamori and Allen, 1986; Wang and Kuo, 1998; Wang,
66 2005; Sieh et al., 2008) or from modeling (Wang, 1995, 1996; Ward, 1996, 2000;
67 Wang and Hwang, 2001). Kanamori and Allen (1986) observed that faults with longer
68 T_R are stronger than those with shorter T_R . Davies et al. (1989) proposed that the
69 longer it has been since the last earthquake, the longer the expected time till the next.
70 Wang and Kuo (1998) observed that for $M \geq 7$ earthquakes in Taiwan T_R strongly
71 follows the Poissonian processes. Enescu et al. (2008) found that the distribution of
72 T_R can be described by an exponential function. From the estimated values of T_R of
73 earthquakes happened on the Chelungpu fault in central Taiwan from trenching data,
74 Wang (2005) found that the earthquakes occurred non-periodically.



75 In order to interpret earthquake recurrences, Shimazaki and Nakata (1980)
76 proposed three simple phenomenological models. Each model has a constantly
77 increasing tectonic stress that is controlled by a critical stress level, σ_c , for failure and
78 a base stress level, σ_b . The three models are: (1) the perfectly periodic model (with
79 constant σ_c , σ_b , and $\Delta\sigma$); (2) the time-predictable model (with constant σ_c , variable
80 σ_b , and variable $\Delta\sigma$); and (3) the slip-predictable model (with variable σ_c , constant σ_b ,
81 and variable $\Delta\sigma$). For the first model, both T_R and D of next earthquake can be
82 predicted from the values of T_R or D of previous ones. For the second model, T_R of
83 next earthquake can be predicted from the values of D of previous ones. For the third
84 model, D of next earthquake can be predicted from the values of T_R of previous ones.
85 However, debates about the three models have been made for a long time. Some
86 examples are given below. Ando (1975) suggested that the second model worked for
87 post-1707 events, yet not for pre-1707 ones in the Nankaido trough, Japan. Wang
88 (2005) assumed that the second model could describe the earthquakes occurred on the
89 Chelungpu fault, Taiwan in the past 1900 years. For the Parkfield earthquake
90 sequence, Bakun and McEvilly (1984) took different models; while Murray and
91 Segall (2002) considered the failure of the second model. From laboratory results,
92 Rubinstein et al. (2012) assumed the failure of the time- and slip-predictable models
93 for earthquakes.

94 Some models, for instance the crack model and dynamical spring-slider model,
95 have been developed for fault dynamics, even though the seismologists have not a
96 comprehensive model. There are several factors in controlling fault dynamics and
97 earthquake ruptures (see Bizzarri, 2009; Wang, 2017b). Among the factors, friction
98 (Nur, 1978; Belardinelli and Belardinelli, 1996) and viscosity (Jeffreys, 1942; Spray,
99 1993; Wang, 2007) are two significant ones.



100 Modeling earthquake recurrence based on different models has been long made and
101 is reviewed by Bizzarri (2012a,b) and Franović et al. (2016). Among the models, the
102 spring-slider model has been used to study fault dynamics and earthquake physics
103 (see Wang 2008). Burridge and Knopoff (1967) proposed the one-dimensional
104 N-body model (abbreviated as the 1-D BK model henceforth). Wang (2000, 2012)
105 extended the 1-D model to 2-D one. The one-, two-, three-, and few-body models with
106 various friction laws have also been applied to approach fault dynamics (see Turcotte,
107 1992). The studies for various friction laws based on spring-slider models are briefly
108 described below: (1) for rate- and state-dependent friction (e.g., Rice and Tse, 1986;
109 Ryabov and Ito, 2001; Erickson et al., 2008, 2011; He et al., 2003; Mitsui and
110 Hirahara, 2009; Bizzarri, 2012a; Abe and Kato, 2013; Kostić et al., 2013a; Bizzarri
111 and Crupi, 2014; Franović et al., 2016); (2) for velocity-weakening friction (e.g.,
112 Carlson and Langer, 1989; Huang and Turcotte, 1992; Brun and Gomez, 1994; Wang
113 and Hwang, 2001; Wang, 2003; Kostić et al., 2013b); (3) for simple static/dynamic
114 friction (e.g., Abaimov et al., 2007; Hasumi, 2007).

115 Some results concerning earthquake recurrence are simply explained below.
116 Erickson et al. (2008) suggested that aperiodicity in earthquake dynamics is due to
117 either the nonlinear friction law (Huang and Turcotte, 1990) or the heterogeneous
118 stress distribution (Lapusta and Rice, 2003). Wang and Hwang (2001) emphasized the
119 importance of heterogeneous frictional strengths. Mitsui and Hirahara (2009) pointed
120 out the effect of thermal pressurization. Dragoni and Piombo (2011) found that
121 variable strain rate causes aperiodicity of earthquakes. Bizzarri and Crupi (2014)
122 found that T_R is dependent on the loading rate, effective normal stress, and
123 characteristic distance of the rate- and state-dependent friction law.



124 As mentioned previously, numerous studies have been made for exploring the
125 frictional effect on earthquake recurrence. But, the study concerning the viscous effect
126 on earthquake recurrence is rare. In the followings, we will investigate the effects of
127 slip-weakening friction due to thermal-pressurization and viscosity on earthquake
128 recurrence based on the one-body spring-slider model.

129

130 **2 One-body Model**

131 Fig. 2 displays the one-body spring-slider model. In the model, m , K , N , F , η , u , v
132 ($=du/dt$), v_p , and $u_o=v_p t$ denote, respectively, the mass of the slider, the stiffness (or
133 spring constant) of the leaf spring, the normal force, the frictional force between the
134 slider and the moving plate, the damping coefficient (to represent viscosity as
135 explained below), the displacement of the slider, the velocity of the slider, the plate
136 moving speed, and the equilibrium location of the slider. The frictional force F (with
137 the static value of F_o) is usually a function of u or v . Viscosity results in the viscous
138 force, Φ , between the slider and the moving plate, and Φ is in terms of v . A driving
139 force, $Kv_p t$, caused by the moving plate through the leaf spring pulls the slider to
140 move. The equation of motion of the model is:

141

$$142 \quad md^2u/dt^2 = -K(u-u_o) - F(u,v) - \Phi(v). \quad (1)$$

143

144 When $Kv_p t \geq F_o$, F changes from static frictional force to dynamic one and thus makes
145 the slider move.

146 The frictional force $F(u,v)$ is controlled by several factors (see Wang, 2016; and
147 cited references therein). An effect combined from temperature and fluids in a fault
148 zone can result in thermal pressurization (abbreviated as TP below) which would yield



149 a shear stress (resistance) on the fault plane (Sibson, 1973; Lachenbruch, 1980; Rice,
150 2006; Wang, 2009, 2011, 2016, 2017a,b,c; Bizzarri, 2009). Rice (2006) proposed two
151 end-member models of TP, i.e., the adiabatic-undrained-deformation (AUD) model
152 and slip-on-a-plane (SOP) model. The latter is not appropriate in this study because of
153 the request of constant velocity. The former is related to a homogeneous simple strain
154 ε at a constant normal stress σ_n on a spatial scale of the sheared layer. Its shear
155 stress-slip function, $\tau(u)$, is: $\tau(u)=f(\sigma_n-p_o)\exp(-u/u_c)$ (Rice, 2006), which decreases
156 exponentially with increasing u . The characteristic displacement is $u_c=\rho_f C_v h/\mu_f A$,
157 where ρ_f , C_v , h , μ_f , and A are, respectively, the fluid density, heat capacity (in
158 J^oC/kg), the thickness, frictional strength, and the undrained pressurization factor of
159 the fault zone.

160 Based on the AUD model, Wang (2009, 2016, 2017a,b,c) took a simplified slip-
161 weakening friction law (denoted by the TP law hereafter):

162

$$163 \quad F(u)=F_o\exp(-u/u_c). \quad (2)$$

164

165 An example of the plot of $F(u)$ versus u for five values of u_c , i.e., 0.1, 0.3, 0.5, 0.7,
166 and 0.9 m, which are taken from Wang (2016), is displayed in Fig. 3. $F(u)$ decreases
167 with increasing u and its decreasing rate, γ , decreases with increasing u_c . The force
168 drop is lower for larger u_c than for smaller u_c . When $u \ll u_c$, $\exp(-u/u_c) \approx 1-u/u_c$, thus
169 indicating that u_c^{-1} is almost γ at small u . This TP law is used in this study.

170 A detailed description about viscosity and the viscous force $\Phi(v)$ can be found in
171 Wang (2016), and only a brief explanation is given below. Jeffreys (1942) first and
172 then numerous authors (Byerlee, 1968; Turcotte and Schubert, 1982; Scholz, 1990;
173 Rice et al., 2001; Wang, 2016) emphasized the viscous effect on faulting due to



174 frictional melts. The viscosity coefficient, ν , of rocks is influenced by T (see Turcotte
175 and Schubert, 1982; Wang, 2011). Spray (2005; and cited references therein) observed
176 a decrease in ν with increasing T . He also stressed that frictional melts with low ν
177 could produce a large volume of melting, thus reducing the effective normal stress.
178 This behaves like fault lubricants during seismic slip.

179 The physical models of viscosity can be found in several articles (e.g., Cohen, 1979;
180 Hudson, 1980). The stress–strain relationship is $\sigma = E\varepsilon$ where σ and E are, respectively,
181 the stress and the elastic modulus for an elastic body and $\sigma = \nu(d\varepsilon/dt)$, where ν is the
182 viscosity coefficient, for a viscous body. Two simple models with a viscous damper
183 and an elastic spring are often used to describe the viscous materials. A viscous
184 damper and an elastic spring are connected in series leading to the Maxwell model
185 and in parallel resulting in the Kelvin-Voigt model (or the Voigt model). According to
186 Hudson (1980), Wang (2016) proposed that the latter is more suitable than the former
187 for seismological problems and thus the Kelvin-Voigt model, whose constitution law
188 is $\sigma(t) = E\varepsilon(t) + \nu d\varepsilon(t)/dt$, is taken here and displayed in Fig. 2. The viscous stress is νv .

189 In order to investigate the viscous effect in a dynamical system, Wang (2016)
190 defined the damping coefficient, η , based on the phenomenon that an oscillating body
191 damps in viscous fluids. According to Stokes' law, $\eta = 6\pi R\nu$ for a sphere of radius R in
192 a viscous fluid of ν (see Kittel et al., 1968). Hence, the viscous force in Equation 1 is
193 represented by $\Phi = \eta v$. Note that the unit of η is N(m/s)^{-1} .

194 Some authors (Knopoff et al., 1973; Cohen, 1979; Rice, 1993; Xu and Knopoff,
195 1994; Knopoff and Ni, 2001; Bizzarri, 2012a; Dragoni and Santini, 2015) considered
196 that viscosity plays a role on causing seismic radiation to release strain energy during
197 faulting.

198



199 3 Normalization of Equation of Motion

200 Putting Eq. 2 and $\Phi = \eta v$ into Eq. 1 leads to

201

$$202 \quad m d^2 u / dt^2 = -K(u - v_p t) - F_o \exp(-u/u_c) - \eta v. \quad (3)$$

203

204 Eq. 3 is normalized for easy numerical computations based on the normalization

205 parameters, which is dimensionless: $D_o = F_o / K$, $\omega_o = (K/m)^{1/2}$, $\tau = \omega_o t$, $U = u / D_o$, and

206 $U_c = u_c / D_o$. The normalized velocity, acceleration, and driving velocity are $V = dU/d\tau =$

207 $[F_o / (mK)^{1/2}]^{-1} du/dt$, $A = d^2 U / d\tau^2 = (F_o / m)^{-1} d^2 u / dt^2$, and $V_p = v_p / (D_o \omega_o)$, respectively.

208 Define $\Omega = \omega / \omega_o$ to be the dimensionless angular frequency, and thus the phase ωt

209 becomes $\Omega \tau$. For the purpose of simplification, $\eta / (mK)^{1/2}$ is denoted by η below.

210 Substituting all normalization parameters into Eq. 3 leads to

211

$$212 \quad d^2 U / d\tau^2 = -U - \eta dU/d\tau \exp(-U/U_c) + V_p \tau. \quad (4)$$

213

214 In order to numerically solve Eq. (4), we define two new parameters, i.e., $y_1 = U$ and

215 $y_2 = dU/d\tau$. Eq. 4 can be re-written as two first-order differential equations:

216

$$217 \quad dy_1/d\tau = y_2 \quad (5a)$$

218

$$219 \quad dy_2/d\tau = -y_1 - \eta y_2 \exp(-y_1/U_c) + V_p \tau. \quad (5b)$$

220

221 We can numerically solve Eq. 5 by using the fourth-order Runge-Kutta method (Press

222 et al., 1986). Because of $v_p \approx 10^{-10}$ m/s, V_p must be much smaller than 1. To shorten the



223 computational times, V_p is taken to be 10^{-2} . The backward slip is not allowed in the
224 simulations, because of common behavior of forward earthquake ruptures.

225 A phase portrait, which is a plot of a physical quantity, y , versus another, x , i.e.,
226 $y=f(x)$, is commonly used to represent nonlinear behavior of a dynamical system
227 (Thompson and Stewart, 1986). The intersection point between $f(x)$ and the bisection
228 line of $y=x$, is defined as the fixed point, that is, $f(x)=x$. If $f(x)$ is continuously
229 differentiable in an open domain near a fixed point x_f and $|f'(x_f)|<1$, attraction can
230 appear at the fixed point. Chaos can also be generated at some attractors. The details
231 can be seen in Thompson and Stewart (1986). In this study, the phase portrait is the
232 plot of V/V_{max} versus U/U_{max} .

233

234 **4 Simulation Results**

235 The results of numerical simulations are shown in Figs. 4–12. The temporal
236 variations in V/V_{max} (displayed by thin solid lines) and cumulative slip $\Sigma U/U_{max}$
237 (displayed by solid lines) are displayed in the left-handed-side panels; while the phase
238 portraits of V/V_{max} versus U/U_{max} (displayed by solid lines) are shown in the right-
239 handed-side panels. Because the maximum values of both V and U decrease from case
240 (a) to case (d), denote the maximum velocity and maximum displacement for case (a)
241 of each figure are denoted by, respectively, V_{max} and U_{max} which are taken as a factor
242 in scaling the waveforms from case (a) to case (d). In the right-handed-side panels of
243 Figs. 4–12, the dashed line represents the bisection line.

244 The cases not including the viscous effect, i.e., $\eta=0$, are first simulated and results
245 are shown in Fig. 4 for four values of U_c : (a) for $U_c=0.2$; (b) for $U_c=0.4$; (c) for
246 $U_c=0.8$; and (d) for $U_c=1.0$. The results of the cases including viscosity, i.e., $\eta\neq 0$, are
247 displayed in Figs. 5–7 for four values of η : (a) for $\eta=0.20$; (b) for $\eta=0.40$; (c) for



248 $\eta=0.6$; and (d) for $\eta=0.8$. The values of U_c are 0.20 in Fig. 5, 0.50 in Fig. 6, and 0.80
249 in Fig. 7.

250 Figs. 4–7 show that when U_c and η are constants during the computational time
251 periods, the general patterns of temporal variations in cumulated slip do not change.
252 Some of the previous studies suggest that the patterns of temporal variations in
253 cumulated slip can change with time. The changes of U_c and η with time should play
254 the main roles. From $u_c = \rho_f C v h / \mu_f A$ of the TP model (see Rice 2006), the width of the
255 slipping zone, h , where the maximum deformation is concentrated (Bizzarri, 2009), is
256 a significant parameter in this study. The reasons to select h to be the main factor are
257 explained below in the section of “Discussion.”. From geological surveys, Rathbun
258 and Marone (2010) observed that h is not spatially uniform even within a single fault.
259 Hull (1988) and Marrett and Allmendinger (1990) found that the wear processes
260 occurring during faulting could widen h , and thus h could vary with time. According
261 to the results gained by several authors (e.g., Power et al., 1988; Robertson, 1983; and
262 Bizzarri, 2010), Bizzarri (2012b) assumed that h is linearly dependent on the
263 cumulated slip, $S(t) = \sum D(t)$, and can be represented by $h(t) = CS(t)$ where C is a
264 dimensionless constant. Since u_c is proportional to h and $U_c = u_c / D_o$, U_c is
265 proportional to C . This means that the more mature the fault is, the thicker its slip
266 zone is. Simulation results for four values of C are shown in Figs. 8–12: (a) for
267 $C=0.0001$; (b) for $C=0.001$; (c) for $C=0.01$; and (d) for $C=0.05$ when $U_c=0.1$ and $\eta=0$
268 in Fig. 8, when $U_c=0.5$ and $\eta=0$ in Fig. 9, when $U_c=0.9$ and $\eta=0$ in Fig. 10, when
269 $U_c=0.1$ and $\eta=1$ in Fig. 11, and when $U_c=0.5$ and $\eta=1$ in Fig. 12.

270

271 **5 Discussion**

272 The left-handed-side panels in Fig. 4 with $\eta=0$ show that the peak velocity, V_m , and



273 final slip, D , with the respective maximum values in case (a) as mentioned above, for
274 all simulated events decrease with increasing U_c . From Fig. 3, the force drop, ΔF ,
275 decreases with increasing U_c , thus indicating that larger ΔF yields higher V_m and
276 larger D . This interprets the negative dependence of V_m and D on U_c . The value of τ_D
277 increases with U_c ; while T_R decreases with increasing U_c . When $U_c=1$, V_m and D are
278 both very small and the system behaves like creeping of a fault. In the right-handed-
279 side panels, there are two fixed points: one at $V=0$ and $U=0$ and the other at larger V
280 and larger U . The slope values at the two fixed points decrease with increasing U_c ,
281 thus suggesting that the fixed point is not an attractor for small U_c and can be an
282 attractor for larger U_c . The phase portrait for $U_c=1$ is very tiny, because the final slip
283 for $U_c=1.0$ is much smaller than those for $U_c=0.2, 0.4$, and 0.8 . Hence, $U_c=1$ will not
284 be taken into account in the following simulations.

285 The left-handed-side panels in Figs. 5–7 show that V_m and D decrease when either
286 U_c or η increases; while τ_D increases with η and U_c . Meanwhile, T_R increases when
287 either η increases or U_c decreases. The right-handed-side panel exhibits that the
288 phase portraits are coincided for all simulated events for a certain η . There are two
289 fixed points for each case: one at $V=0$ and $U=0$ and the other at larger V and larger U .
290 The slope values at the two fixed points decrease when either U_c or η increases. This
291 suggests that the fixed point is not an attractor for small U_c and low η , and can be an
292 attractor for large U_c and high η . Clearly, the final slip is shorter for $U_c=0.9$ than for
293 $U_c=0.1$ and 0.5 .

294 From Figs. 5–7, we can see that the temporal variation in cumulative slip can be
295 described by the perfectly periodic model as mentioned above. Hence, when U_c and η
296 do not change with time, the rate of cumulative slip retains a constant in the
297 computational time period. This is similar to the simulation results with the periodical



298 earthquake occurrences obtained by some authors (e.g., Rice and Tse, 1986; Ryabov
299 and Ito, 2001; Erickson et al., 2008; Mitsui and Hirahara, 2009) based on the
300 one-body model with rate- and state-dependent friction or velocity- weakening
301 friction. But, the present result is inconsistent with the simulation results, from which
302 either the time-predictable model or the slip-predictable model cannot interpret the
303 temporal variation in cumulative slip, based on the same model obtained by others
304 (e.g., He et al., 2003; Bazzarri 2012b; Bizzarri and Crupi, 2014; Kostić et al., 2013a,b;
305 Franović et al., 2016). The differences between the two groups of researchers might
306 be due to distinct additional constrains in respective studies. Although the detailed
307 discussion of such differences is important and significant, it is out of the scope of this
308 study and ignored here.

309 The phase portraits shown in the right-handed-side panels of Figs. 5–7 exhibit that
310 the period related to T_R and the size associated with D decrease with increasing h .
311 This is similar to that obtained from the left-handed-side panels. There are two fixed
312 points for each case: one at larger V and larger U and the other at $V=0$ and $U=0$. The
313 slope values of the fixed point at larger V and larger U are higher than 1 and decreases
314 with increasing η . This means that larger η is easier to generate chaos than small η .
315 However, the reducing rate of slope value decreases with increasing U_c . The slope
316 values of the fixed point at $V=0$ and $U=0$ are higher than 1 and only decrease with
317 increasing η . This suggests that the fixed points at $V=0$ and $U=0$ can be an attractor.
318 This behavior becomes weaker when U_c increases.

319 The previous study demonstrates that when U_c and η are constants during the
320 computational time periods, the general patterns of temporal variations in cumulated
321 slip cannot change. In order to investigate the effects on the patterns of temporal
322 variations in cumulated slip, we must consider changes of U_c and η with time. The



323 viscosity coefficient can actually vary immediately before and after the occurrence of
324 an earthquake (see Spray, 1883, 2005; Wang, 2017b,c). But, a lack of long-term
325 variation in η does not allow us to explore its possible effect on the change of general
326 patterns of temporal variations in cumulated slip. Here, only the possible effect due to
327 time-varying U_c .

328 As mentioned above, U_c is u_c/D_o and thus $U_c = \rho_f C_v h / \mu_f D_o A$, where $A =$
329 $(\lambda_f - \lambda_n) / (\beta_f + \beta_n)$ (Rice, 2006). Obviously, U_c is controlled by six factors, i.e., ρ_f , C_v , h ,
330 μ_f , D_o , and A . Since the tectonics of a region is generally stable during a long time,
331 the value of $D_o = F_o / K$ could not change too much and thus would not influence U_c .
332 The Debye law (cf. Reif, 1965) gives $C_v \sim (T + 273.16)^3$, where 273.16 is the value to
333 convert temperature from Celsius to Kelvin, at low T and $C_v \approx \text{constant}$ at high T . The
334 threshold temperature, from which C_v begins to approach a constant, is 200–300 °K.
335 In this study, C_v is almost a constant because of $T > 250$ °C = 523.16 °K, which is the
336 average ambient temperature of fault zone with depths ranging from 0 to 20 km.
337 Hence, C_v is almost constant during a long time and thus cannot influence U_c .

338 The frictional strength, μ_f , is influenced by several factors including humidity,
339 temperature, sliding velocity, strain rate, normal stress, thermally activated rheology
340 etc (Marone, 1998; Rice, 2006), and thus can change with time (Sibson, 1992; Rice,
341 2006). Hirose and Bystricky (2007) observed that serpentine dehydration and
342 subsequent fluid pressurization due to co-seismic frictional heating may reduce μ_f and
343 thus promote further weakening in a fault zone. The pore fluid pressure exists in wet
344 rocks, yet not in dry rocks. Clearly, the time variation in μ_f can affect the earthquake
345 recurrences. However, a lack of long-term observations of μ_f during a seismic cycle
346 makes the studies of its effect on earthquake recurrence be impossible.

347 The fluid density ρ_f and the porosity n depend on T and p . Although there are



348 numerous studies on such dependence (Lachenbruch, 1980; Bizzarri, 2012b; and cited
349 references therein), observed data and theoretical analyses about the values of p_f and n
350 during a seismic cycle are rare.

351 The porosity is associated with the permeability, κ . Bizzarri (2012c) pointed out
352 that the time-varying permeability, $\kappa(t)$, and porosity of a fault zone (cf. Mitsui and
353 Cocco, 2010; Bizzarri, 2012b) can reduce T_R . One of the Kozeny–Carman's (KC)
354 relations (Costa, 2006; and references cited therein) is: $\kappa(t) = \kappa_C \phi^2(t) d^3(t) / [1 - \phi(t)]^2$,
355 where κ_C is a dimensionless constant depending on the material in consideration; ϕ is
356 V_{voids}/V_{tot} where V_{voids} and V_{tot} are, respectively, the pore volume and the total volume
357 of the porous materials; and d is the (average) diameter of the grains, ranging between
358 4×10^{-5} m and 1×10^{-4} m (Niemeijer et al., 2010). Usually, κ , ϕ , and d can vary in the
359 fault zone (Segall and Rice, 1995). After faulting κ and ϕ would change and d
360 becomes smaller because of refining of the grains. According to this relation, Bizzarri
361 (2012b) found that $\kappa(t)$ could significantly reduce T_R in comparison with the base
362 model with constant κ . The reason is explained below. The time-varying permeability
363 can result in the time-varying pore pressure, p_f . This can reduce the frictional
364 resistance from $\tau = \mu(\sigma_n - p_f)$ and thus could trigger earthquakes earlier. Hence, the
365 time-varying permeability can change T_R . Nevertheless, we cannot investigate its
366 influence on earthquake recurrence here because there is a lack of a long-term
367 observation of hydraulic parameters during a seismic cycle.

368 It is significant to explore the factors that can yield a non-perfectly periodic seismic
369 cycle. The width of the slipping zone, h , can be a candidate as pointed out by some
370 authors (e.g., Bizzarri, 2009; Rathbun and Marone, 2010). Since the displacement
371 along a fault is controlled by the fault rheology, h should depend on the rheology on
372 the sliding interface. The wear processes occurring during faulting could widen h



373 (Hull, 1988; Marrett and Allmendinger, 1990). According to the results gained by
374 several authors (e.g., Power et al., 1988; Robertson, 1983; and Bizzarri, 2010),
375 Bizzarri (2012b) proposed a linear dependence of h on the cumulated slip, $S(t)=\sum D(t)$,
376 i.e., $h(t)=CS(t)$ where C is a dimensionless constant. When the slip zone is thicker, the
377 fault should be more mature. Since U_c is a function of h , $U_c=uc/D_o=\rho_f C_v h/\mu_f A D_o$ is
378 also proportional to C and thus U_c increases with C . Hence, numerical simulations for
379 various values of C and the results are shown in Figs. 8–12, which are different from
380 Figs. 4–8 especially for large C .

381 The left-handed-side panels of Figs. 8–12 show that V_m , D , τ_D , and T_R are all
382 similar when $C \leq 0.001$; while their values are larger for $C=0.01$ than for $C=0.05$ and
383 also decrease with time. A decrease in D is particularly remarkable when $C \geq 0.01$.
384 When $C=0.05$ or h is wider than a critical value, normal earthquakes cannot occur and
385 only creeping can happen. Obviously, T_R decreases with increasing C , thus leading to
386 an decrease in T_R with increasing h . This is similar to the result obtained by Bizzarri
387 (2010; 2012b). As mentioned above, the fault should be more mature when the slip
388 zone is thicker. Consequently, both T_R and D decrease when the fault becomes more
389 mature. This might suggest that it is more difficult to produce large earthquakes along
390 a fault when it becomes more mature. This implicates that seismic hazard is higher for
391 a young fault than a mature one. This sounds physically reasonable. Meanwhile,
392 either the time- or slip- predictable model can only describe the temporal variations of
393 cumulative slip in the earlier time period, yet not in the later one.

394 The right-handed-side panels of Figs. 8–12 exhibit that the phase portraits for
395 $C=0.001$ are slightly different from those for $C=0.0001$ even though the patterns of
396 their variations in V and U are similar; while the phase portraits for $C > 0.001$ are
397 different from those for $C \leq 0.001$. An increase in h due to an increase in C with



398 cumulative slip enlarges U_c . This can be explained from Fig. 3 which shows that
399 larger U_c yields a lower ΔF than smaller U_c . Hence, an increase in U_c produces a
400 decrease in ΔF , thus resulting in low V_m and small D . In addition, An increase in U_c
401 makes $\exp(-U/U_c)$ approach unity, especially for small U , thus reducing the nonlinear
402 effect caused by TP friction.

403 Unlike Figs. 4–7, the size of phase portraits in the right-handed-side panels of Figs.
404 8–12 decreases with increasing C . This reflects a decrease in T_R and D of events with
405 increasing C as mentioned previously. In the phase portraits, there are two fixed
406 points for each case: one at larger V and larger U and the other at $V=0$ and $U=0$. The
407 slope values at the fixed point at larger V and larger U are higher than 1 and only
408 slightly decreases with time when $C \leq 0.01$; while the values remarkably decrease with
409 time when $C=0.05$. The slope values at the fixed point at $V=0$ and $U=0$ are higher than
410 1 and only slightly decreases with time when $C \leq 0.01$; while those decrease with time
411 and finally approaches unity when $C=0.05$. Results suggest that the fixed points at
412 larger V and larger U for all cases in study are not an attractor; and those at $V=0$ and
413 $U=0$ can evolve to an attractor with time when $C=0.05$. The phenomenon for $C=0.05$
414 is more remarkable and the evolution is faster for large U_c than for small U_c .

415

416 **6 Conclusions**

417 To study the frictional and viscous effects on earthquake recurrence, numerical
418 simulations of the temporal variations in cumulative slip have been conducted based
419 on the normalized equation of a one-body model in the presence of thermal-
420 pressurized slip-weakening friction and viscosity. The major model parameters of
421 friction and viscosity are represented, respectively, by U_c and η , where $U_c=u_c/D_o$ is
422 the normalized characteristic distance and η is the normalized damping coefficient.



423 Numerical simulation of the time variations in V/V_{max} and cumulative slip $\Sigma U/U_{max}$,
424 the phase portrait of V/V_{max} versus U/U_{max} , and the phase portrait of $\exp(-U/U_c)$ versus
425 U/U_{max} are made for various values of U_c and η .

426 Results exhibit that both friction and viscosity remarkably affect earthquake
427 recurrence. The recurrence time, T_R , increase when η increases or U_c decreases. The
428 final slip, D , and the duration time of slip, τ_D , of an event slightly decrease when η or
429 τ_D increases and slightly increases with U_c . Considering the effect due to wear process,
430 the thickness of slip zone, h that depends on the cumulated slip, $S(t)=\Sigma D(t)$, i.e.,
431 $h(t)=CS(t)$ (C =a dimensionless constant), is an important factor in influencing
432 earthquake recurrences. Because of $U_c=\rho_f C_v h/\mu_f A D_o$, U_c increases with C . When
433 $C>0.0001$, the wear process influences the recurrence of slip and the effect increases
434 with C . When the slip zone is thicker, the fault should be more mature and T_R
435 increases. Hence, both T_R and D decrease when the fault becomes more mature. This
436 might suggest that it is more difficult to produce large earthquakes along a fault when
437 it becomes more mature. The temporal variation in slip cannot be interpreted by the
438 time-predictable or slip-predictable model when the fault is affected by wear process
439 with large C . In addition, the size of phase portrait of V/V_{max} versus U/U_{max} decreases
440 with increasing C . This reflects a decrease in T_R and D of events with increasing C as
441 inferred from the temporal variations in cumulative slip.

442

443

444 **Acknowledgments** The study was financially supported by Academia Sinica and
445 the Ministry of Science and Technology (Grant No.: MOST-106-2116-M-001-005).

446



447 **References**

- 448 Abaimov, S.G., Turcotte D.L., Shcherbakov R., and Rundle J.B.: Recurrence and
449 interoccurrence behavior of self-organized complex phenomena, *Nonlin.*
450 *Processes Geophys.*, 14, 455-464, 2007
- 451 Abe, Y. and Kato N.: Complex earthquake cycle simulations using a two-degree-
452 of-freedom spring-block model with a rate- and state-friction law, *Pure. Appl.*
453 *Geophys.*, 170, 745-765, 2013.
- 454 Ando, M.; Source mechanisms and tectonic significance of historic earthquakes along
455 the Nankai trough, Japan, *Tectonophys.*, 27, 119-140, 1975
- 456 Bakun, W.H. and McEvilly T.V.: Earthquakes near Parkfield, California: comparing
457 the 1934 and 1966 sequences, *Science*, 205, 1375-1377, 1979.
- 458 Bakun, W.H. and McEvilly T.V.: Recurrence models and Parkfield, California,
459 earthquakes, *J. Geophys. Res.*, 89, 3051-3058, 1984.
- 460 Beeler, N.M., Lockner D.L., and Hickman S.H.: A simple stick-slip model for
461 repeating earthquakes and its implication for microearthquakes at Parkfield, *Bull.*
462 *Seism. Soc. Am.*, 91(6), 1797-1804, 2001.
- 463 Belardinelli, M.E. and Belardinelli E.: The quasi-static approximation of the
464 spring-slider motion. *Nonl. Processes Geophys.*, 3, 143-149, 1996.
- 465 Bizzarri, A.: What does control earthquake ruptures and dynamic faulting? A review
466 of different competing mechanism, *Pure. Appl. Geophys.*, 166, 741-776, 2009.
- 467 Bizzarri, A.: On the recurrence of earthquakes: Role of wear in brittle faulting,
468 *Geophys. Res., Letts.*, 37, L20315, <http://dx.doi.org/10.1029/2010GL045480>,
469 2010.
- 470 Bizzarri, A.: Modeling repeated slip failures on faults governed by slip- weakening
471 friction, *Bull. Seism. Soc. Am.*, 102(2), 812-821 doi:10.1785/0120110141, 2012a.



- 472 Bizzarri, A.: What can physical source models tell us about the recurrence time of
473 earthquakes?, *Earth-Sci. Rev.*, 115, 304-318 [http://dx.doi.org/10.1016/j.earscirev.](http://dx.doi.org/10.1016/j.earscirev.2012.10.004)
474 [2012.10.004](http://dx.doi.org/10.1016/j.earscirev.2012.10.004), 2012b
- 475 Bizzarri., A.: Effects of permeability and porosity evolution on simulated earthquakes,
476 *J. Struct. Geol.*, 38, 243-253, <http://dx.doi.org/10.1016/j.jsg.2011.07.009>, 2012c
- 477 Bizzarri, A. and Crupi P.: Linking the recurrence time of earthquakes to source
478 parameters: A dream or a real possibility?, *Pure. Appl. Geophys.*, 171, 2537-2553,
479 DOI:10.1007/s00024-013-0743-1, 2014.
- 480 Brun, J.L. and Gomez A.B.: A four-parameter, two degree-of-freedom block-spring
481 model: Effect of the driver velocity, *Pure. Appl. Geophys.*, 143(4), 633-653, 1994.
- 482 Burridge, R. and Knopoff L.: Model and theoretical seismicity, *Bull. Seism. Soc. Am.*,
483 57, 341-371, 1967.
- 484 Byerlee, J.D.: Brittle-ductile transition in rocks, *J. Geophys. Res.*, 73, 4711-4750,
485 1968.
- 486 Carlson, J.M. and Langer J.S: Mechanical model of an earthquake fault, *Phys. Rev. A*,
487 40, 6470-6484, 1989.
- 488 Chen, K.H., Nadeau R.M., and Rau R.J.: Towards a universal rule on the recurrence
489 interval scaling of repeating earthquakes?, *Geophys. Res., Letts.*, 34, L16308,
490 doi:10.1029/2007GL030554, 2007.
- 491 Cohen, S.: Numerical and laboratory simulation of fault motion and earthquake
492 occurrence, *Rev. Geophys. Space Phys.*, 17(1), 61-72, 1979.
- 493 Costa, A.: Permeability-porosity relationship: a reexamination of the Kozeny-
494 Carman equation based on a fractal pore-space geometry assumption, *Geophys.*
495 *Res. Letts.*, 33, L02318 <http://dx.doi.org/10.1029/2005GL025134>, 2006.
- 496 Davis, P.M., Jackson D.D., and Kagan Y.Y.: The longer it has been since the last



- 497 earthquake, the longer the expected time till the next?, *Bull. Seism. Soc. Am.*,
498 79:1439-1456, 1989.
- 499 Dragoni, M. and Piombo A.: Dynamics of a seismogenic fault subject to variable
500 strain rate, *Nonlin. Processes Geophys.*, 18, 431-439, doi:10.5194/npg-18-431-
501 2011, 2011.
- 502 Dragoni, M. and Santini S.: A two-asperity fault model with wave radiation,
503 *Phys. Earth Planet. Inter.*, 248, 83-93, 2015.
- 504 Enescu, B., Struzik Z., and Kiyono K.: On the recurrence time of earthquakes: insight
505 from Vrancea (Romania) intermediate-depth events, *Geophys. J. Int.*, 172, 395-
506 404, doi:10.1111/j.1365-246X.2007.03664.x, 2008.
- 507 Erickson, B., Birnir B., and Lavallée D.: A model for aperiodicity in earthquakes,
508 *Nonlin. Processes Geophys.*, 15, 1-12, 2008.
- 509 Erickson, B., Birnir B., and Lavallée D.: Periodicity, chaos and localization in a
510 Burridge–Knopoff model of an earthquake with rate-and-state friction, *Geophys.*
511 *J. Int.*, 187, 178-198, doi:10.1111/j.1365-246X.2011.05123.x, 2011.
- 512 Franović, I., Kostić S., Perc M., Klinshov V., Nekorkin V., and Kurths J.: Phase
513 response curves for models of earthquake fault dynamics, *Chaos*, 26, 063105,
514 <http://dx.doi.org/10.1063/1.4953471>, 2016.
- 515 Hasumi, T.: Interoccurrence time statistics in the two-dimensional Burridge–Knopoff
516 earthquake model, *Phys. Rev. E*, 76, 026117, DOI:10.1103/PhysRevE.76.026117,
517 2007.
- 518 He, C., Wong T.f., and Beeler N.M.: Scaling of stress drop with recurrence interval
519 and loading velocity for laboratory-derived fault strength relations, *J. Geophys.*
520 *Res.*, 108(B1), 2037 doi:10.1029/2002JB001890, 2003.
- 521 Hirose, T. and Bystricky M.: Extreme dynamic weakening of faults during



- 522 dehydration by coseismic shear heating, *Geophys. Res., Letts.*, 34, L14311
523 doi:10.1029/2007GL030049, 2007.
- 524 Huang, J. and Turcotte D.L.: Are earthquakes an example of deterministic chaos?,
525 *Geophys. Res., Letts.*, 17(3), 223-226, 1990.
- 526 Huang, J. and Turcotte D.L.: Evidence of chaotic fault interactions in the seismicity of
527 the San Andreas fault and Nankai trough, *Nature*, 348, 234-236, 1992.
- 528 Hudson, J.A.: The excitation and propagation of elastic waves. Cambridge
529 Monographs on Mechanics and Applied Mathematics, Cambridge Univ. Press,
530 226 pp., 1980.
- 531 Hull, J.: Thickness–displacement relationships for deformation zones, *J. Struct. Geol.*,
532 10, 431-435, [http://dx.doi.org/10.1016/0191-8141\(88\)90020-X](http://dx.doi.org/10.1016/0191-8141(88)90020-X), 1988.
- 533 Jeffreys, H.: On the mechanics of faulting, *Geol. Mag.*, 79, 291, 1942.
- 534 Kanamori, H. and Allen C.R.: Earthquake repeating time and average drop, In: Das et
535 al. (eds.) *Earthquake Source Mechanics Maurice Ewing Series 6*, AGU, 227-235,
536 1986.
- 537 Kittel C, Knight WD, Ruderman MA (1968) *Mechanics*. Berkeley Physics Course vol
538 1 McGraw-Hill Book Co New York, 1986.
- 539 Knopoff, L., and Ni X.X.: Numerical instability at the edge of a dynamic fracture,
540 *Geophys. J. Int.*, 147, F1-F6, 2001.
- 541 Knopoff, L., Mouton J.Q., and Burridge R.: The dynamics of a one-dimensional fault
542 in the presence of friction, *Geophys. J. R. astro. Soc.*, 35, 169-184, 1973.
- 543 Kostić, S., Franović I., Todorović K., and Vasović N.: Friction memory effect in
544 complex dynamics of earthquake model, *Nonlin. Dyn.* 73, 1933-1943, DOI:10.
545 1007/s11071-013-0914-8, 2013a.
- 546 Kostić, S., Vasović N., Franović I., and Todorović K.: Dynamics of simple earthquake



- 547 model with time delay and variation of friction strength, *Nonlin. Processes*
548 *Geophys.*, 20, 857-865, doi:10.5194/npg-20-857-2013, 2013b.
- 549 Lachenbruch, A.H.: Frictional heating, fluid pressure, and the resistance to fault
550 motion, *J. Geophys. Res.*, 85, 6097-6122, 1980.
- 551 Lapusta, N. and Rice J.R.: Nucleation and early seismic propagation of small and
552 large events in a crustal earthquake model, *J. Geophys. Res.*, 108, 1-18, 2003.
- 553 Marone, C.: Laboratory-derived friction laws and their application to seismic faulting,
554 *Ann. Rev. Earth Planet. Sci.*, 26, 643-669, 1998.
- 555 Marrett, R. and Allmendinger R.W.: Kinematic analysis of fault-slip data, *J. Struct.*
556 *Geol.*, 12, 973-986, doi.org/10.1016/0191-8141(90)90093-E, 1990.
- 557 Mitsui, Y. and Cocco M.: The role of porosity evolution and fluid flow in frictional
558 instabilities: a parametric study using a spring-slider dynamic system, *Geophys.*
559 *Res., Letts.*, 37, L23305, doi.org/10.1029/2010GL045672, 2010.
- 560 Mitsui, Y. and Hirahara K.: Coseismic thermal pressurization can notably prolong
561 earthquake recurrence intervals on weak rate and state friction faults: numerical
562 experiments using different constitutive equations, *J. Geophys. Res.*, 114,
563 B09304, doi.org/10.1029/2008JB006220, 2009.
- 564 Murray, J. and Segall P.: Testing time-predictable earthquake recurrence by direct
565 measurement of strain accumulation and release, *Nature*, 49, 287-291, 2002.
- 566 Nadeau, R.M. and Johnson L.R.: Seismological studies at Parkfield VI moment
567 release rates and estimates of source parameters for small repeating earthquake,
568 *Bull. Seism. Soc. Am.*, 88, 790-814, 1998.
- 569 Niemeijer, A., Marone C., and Ellsworth D.: Frictional strength and strain weakening
570 in simulated fault gouge: competition between geometrical weakening and
571 chemical strengthening, *J. Geophys. Res.*, 115, B10207, doi.org/10.1029/



- 572 2009JB000838, 2010.
- 573 Nur, A.: Nonuniform friction as a physical basis for earthquake mechanics, *Pure. Appl.*
574 *Geophys.*, 116, 964-989, 1978.
- 575 Okada, T., Matsuzawa T., and Hasegawa A.: Comparison of source areas of
576 M4.8+/-0.1 repeating earthquakes off Kamaishi, NE Japan: are asperities
577 persistent features?, *Earth Planet. Sci. Letts.*, 213(3-4), 361-374, [doi.org/
578 10.1016/S0012-821X\(03000299-1](https://doi.org/10.1016/S0012-821X(03000299-1), 2003.
- 579 Power, W.L., Tullis T.E., and Weeks D.J.: Roughness and wear during brittle faulting,
580 *J. Geophys. Res.*, 93, B12, 15268-15278, doi.org/10.1029/JB093iB12p15268,
581 1988.
- 582 Press, W.H., Flannery B.P., Teukolsky S.A., and Vetterling W.T.: *Numerical Recipes*,
583 Cambridge Univ. Press Cambridge, 1986.
- 584 Rathbun, A.P. And Marone C.: Effect of strain localization on frictional behavior of
585 sheared granular materials, *J. Geophys. Res.*, 115, B01204 [doi.org/10.1029/
586 2009JB006466](https://doi.org/10.1029/2009JB006466), 2010.
- 587 Reid, H.F.: The California earthquake of April 18, 1906, In: Report of the State
588 Investigation Commission 2, Mechanics of the Earthquake Carnegie Inst
589 Washington, D.C., 1910.
- 590 Reif, F.: *Fundamentals of statistical and thermal physics*, McGraw-Hill, New York,
591 651 pp., 1965.
- 592 Rice, J.R.: Spatio-temporal complexity of slip on a fault, *J. Geophys. Res.*, 98, B6,
593 9885-9907, 1993.
- 594 Rice, J.R.: Heating and weakening of faults during earthquake slip, *J. Geophys. Res.*,
595 111, B05311, [doi:10.1029/2005JB004006](https://doi.org/10.1029/2005JB004006), 2006.
- 596 Rice, J.R. and Tse S.T.: Dynamic motion of a single degree of freedom system



- 597 following a rate and state dependent friction law, *J. Geophys. Res.*, 91, B1,
598 521-530, 1986.
- 599 Rice, J.R., Lapusta N., and Ranjith K.: Rate and state dependent friction and the
600 stability of sliding between elastically deformable solids, *J. Mech. Phys. Solids*,
601 49, 1865-1898, 2001.
- 602 Robertson, E.C.: Relationship of fault displacement to gouge and breccia thickness,
603 *Mining Engin.*, 35, 1426-1432, 1983.
- 604 Rubinstein, J.L., Ellsworth W.L., Beeler N.M., Kilgore B.D., Lockner D.A., and
605 Savage H.M.: Fixed recurrence and slip models better predict earthquake
606 behavior than the time- and slip-predictable models: 2. Laboratory earthquakes, *J.*
607 *Geophys. Res.*, 117, B02307, doi:10.1029/2011JB008723, 2012.
- 608 Ryabov, V.B. and Ito K.: Intermittent phase transitions in a slider-spring model as a
609 mechanism for earthquakes, *Pure. Appl. Geophys.*, 158:919-930, 2001.
- 610 Scholz, C.H.: *The Mechanics of Earthquakes and Faulting*. Cambridge Univ. Press
611 Cambridge, 439 pp., 1990.
- 612 Schwartz, D.P. and Coppersmith K.S.: Fault behavior and characteristic earthquakes:
613 examples from the Wasatch and San Andreas fault zones, *J. Geophys. Res.*, 89,
614 5681-5698, 1984.
- 615 Segall, P. and Rice J.R.: Dilatancy, compaction, and slip instability of a
616 fluid-infiltrated fault, *J. Geophys. Res.*, 100, 22155-22171, 1995.
- 617 Shimazaki, K. and Nakata T.: Time-predictable model for large earthquakes, *Geophys.*
618 *Res. Letts.*, 7, 279-282, doi.org/10.1029/GL007i004p00279, 1980.
- 619 Sibson, R.H.: Interaction between temperature and pore-fluid pressure during
620 earthquake faulting and a mechanism for partial or total stress release, *Natural*
621 *Phys. Sci.*, 243, 66-68, 1973.



- 622 Sibson, R.H.: Implications of fault-valve behavior for rupture nucleation and
623 recurrence, *Tectonophys.*, 211,283-293, 1992.
- 624 Sieh, K.: A review of geological evidence for recurrence times of large earthquakes,
625 In: *Earthquake Prediction—An International Review*, Maurice Ewing Series, 4,
626 AGU, 181-207, 1981.
- 627 Sieh, K., Natawidjaja D., Meltzner A.J., Shen C.C., and Cheng H.: Earthquake
628 supercycles inferred from sea-level changes recorded in the corals of West
629 Sumatra, *Science*, 322, 1674-1678, 2008.
- 630 Sykes, L.R. and Quittmeyer R.C.: Repeat times of great earthquakes along simple
631 plate boundaries, In: *Earthquake Prediction—An International Review*, Maurice
632 Ewing Series 4, AGU, 217-247, 1981.
- 633 Spray, J.G.: Viscosity determinations of some frictionally generated silicate melts:
634 Implications for fault zone rheology at high strain rates, *J. Geophys. Res.*, 98, B5,
635 8053-8068, 1983.
- 636 Spray, J.G.: Evidence for melt lubrication during large earthquakes, *Geophys. Res.*,
637 *Letts.*, 32, L07301, doi:10.1029/2004GL022293, 2005.
- 638 Sykes, L.R. and Menke W.: Repeat times of large earthquakes: implications for
639 earthquake mechanics and long-term prediction, *Bull. Seism. Soc. Am.*, 96(5),
640 1569-1596, doi.org/10.1785/0120050083, 2006.
- 641 Thompson., J.M.T. and Stewart H.B.: *Nonlinear Dynamics and Chaos*. John Wiley
642 and Sons, New York, 376 pp., 1986.
- 643 Turcotte, D.L.: *Fractal and Chaos in Geology and Geophysics*, Cambridge Univ. Press,
644 New York, 221 pp., 1992.
- 645 Turcotte, D.L. and Schubert G.: *GEODYNAMICS – Applications of Continuum*
646 *Physics to Geological Problems*, Wiley, 450 pp., 1982



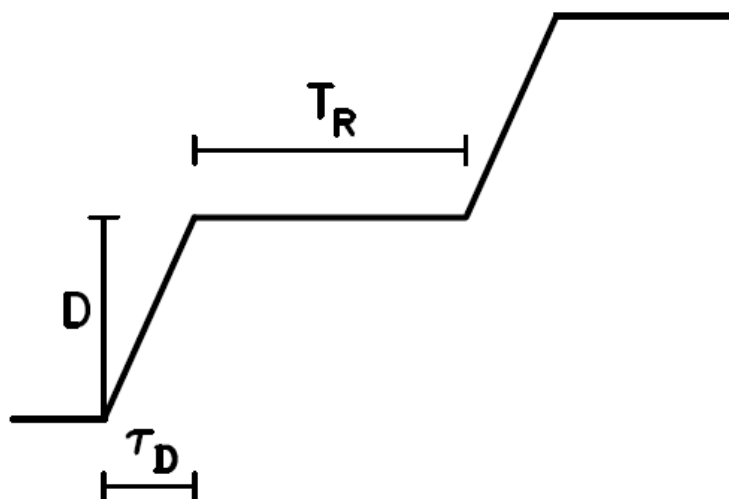
- 647 Wang, J.H.: Effect of seismic coupling on the scaling of seismicity, *Geophys. J. Int.*,
648 121, 475-488, 1995.
- 649 Wang, J.H.: Velocity-weakening friction law as a factor in controlling the
650 frequency-magnitude relation of earthquakes, *Bull. Seism. Soc. Am.*, 86,
651 701-713, 1996.
- 652 Wang, J.H.: Instability of a two-dimensional dynamical spring-slider model of an
653 earthquake fault, *Geophys. J. Int.*, 143, 389-394, 2000.
- 654 Wang, J.H.: A one-body model of the 1999 Chi-Chi, Taiwan, earthquake, *Terr. Atmos.*
655 *Ocean. Sci.*, 14(3), 335-342, 2003.
- 656 Wang, J.H.: Earthquakes rupturing the Chelungpu fault in Taiwan are time-
657 predictable, *Geophys. Res. Lett.*, 32, L06316 doi:10.1029/2004GL021884, 2005.
- 658 Wang, J.H.: A dynamic study of the frictional and viscous effects on earthquake
659 rupture: a case study of the 1999 Chi-Chi earthquake, Taiwan, *Bull. Seism. Soc.*
660 *Am.*, 97(4), 1233-1244, 2007.
- 661 Wang, J.H.: One-dimensional dynamical modeling of earthquakes: A review, *Terr.*
662 *Atmos. Ocean. Sci.*, 19, 183-203, 2008.
- 663 Wang, J.H.: Effect of thermal pressurization on the radiation efficiency, *Bull. Seism.*
664 *Soc. Am.*, 99(4), 2293-2304, 2009.
- 665 Wang, J.H.: Thermal and pore fluid pressure history on the Chelungpu fault at a depth
666 of 1111 meters during the 1999 Chi-Chi, Taiwan, earthquake, *J. Geophys. Res.*,
667 116, B03302 doi:10.1029/2010JB007765, 2011.
- 668 Wang, J.H.: Some intrinsic properties of the two-dimensional dynamical spring-slider
669 model of earthquake faults, *Bull. Seism. Soc. Am.*, 102(2), 822-835, 2012
- 670 Wang, J.H.: Slip of a one-body spring-slider model in the presence of slip-weakening
671 friction and viscosity, *Ann. Geophys.*, 59(5), S0541, DOI:10.4401/ag-7063,



- 672 2016.
- 673 Wang, J.H.: Slip of a two-degree-of-freedom spring-slider model in the presence of
674 slip-weakening friction and viscosity, *Ann. Geophys.*, 60(6), S0659, doi:10.
675 4401/ag-7295, 2017a.
- 676 Wang, J.H.: Frictional and viscous effects on the nucleation phase of an earthquake
677 nucleation, *J. Seismol.*, 21(6), 1517-1539, 2017b.
- 678 Wang, J.H.: Multi-stable slip in a one-degree-of-freedom spring-slider model with
679 thermal-pressurized friction and viscosity, *Nonl. Processes Geophys.*, 24,
680 467-480, doi.org/10.5194/npg-24-467-2017, 2017c
- 681 Wang, J.H. and Hwang R.D.: One-dimensional dynamical simulations of slip
682 complexity of earthquake faults, *Earth Planets Space* 53, 91-100, 2001.
- 683 Wang, J.H. and Kuo C.H.: On the frequency distribution of inter-occurrence times of
684 earthquakes, *J. Seismol.*, 2, 351-358, 1998.
- 685 Ward, S.N.: A synthetic seismicity model for southern California: Cycles,
686 probabilities, and hazard, *J. Geophys. Res.*, 101, 22393-22418, 1996.
- 687 Ward, S.N.: San Francisco Bay Area earthquake simulations: A step toward a
688 standard physical earthquake model, *Bull. Seism. Soc. Am.*, 90, 370-386, 2000.
- 689 Xu, H.J. and Knopoff L.: Periodicity and chaos in a one-dimensional dynamical
690 model of earthquakes, *Phys. Rev. E.*, 50(5), 3577-3581, 1994.
- 691

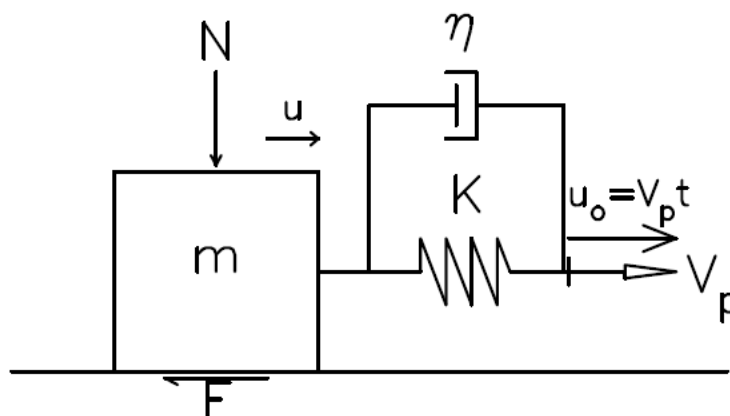


692
693
694



695
696
697
698
699
700
701
702
703

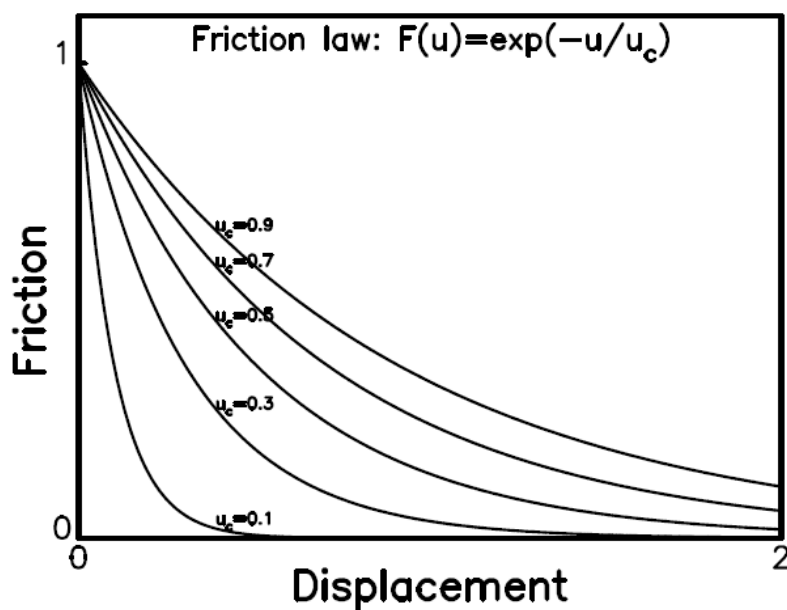
Figure 1. A general pattern of time variation in slip during a seismic cycle: T_R = the recurrence time or the inter-event time of two events in a seismic cycle; τ_D = the duration time of slip of an event; and D = the final slip of an event.



704
705 Figure 2. One-body spring-slider model. In the figure, t , m , K , η , V_p , N , F , u , and u_o
706 denote, respectively, the time, the mass of the slider, the spring constant, the
707 damping coefficient, the driving velocity, the normal force, the frictional force,
708 displacement of the slider, and the equilibrium location of the slider. (after Wang,
709 2016)
710
711



712
713
714
715
716



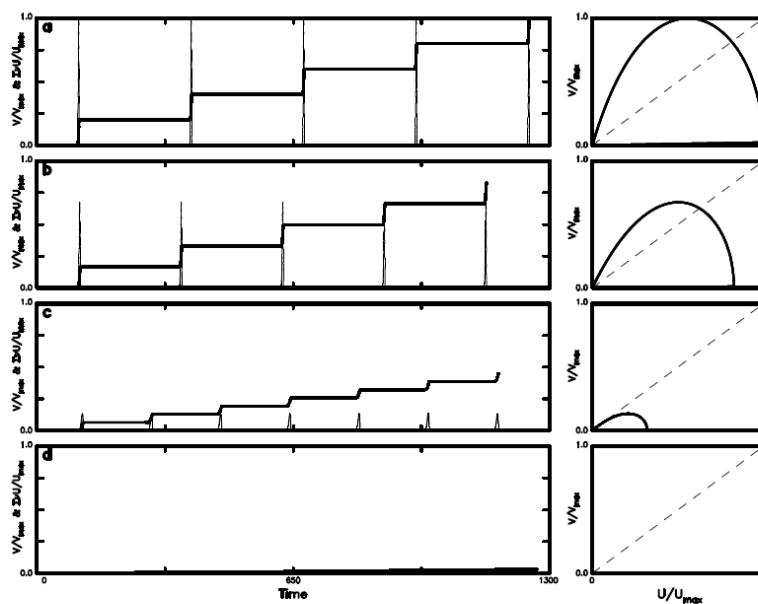
717
718 Figure 3. The plots of $F(u) = \exp(-u/u_c)$ versus u when $u_c = 0.1, 0.3, 0.5, 0.7,$ and 0.9 m.
719 (after Wang, 2016)
720
721



722

723

724



725

726

727

728

729

730

731

732

733

734

735

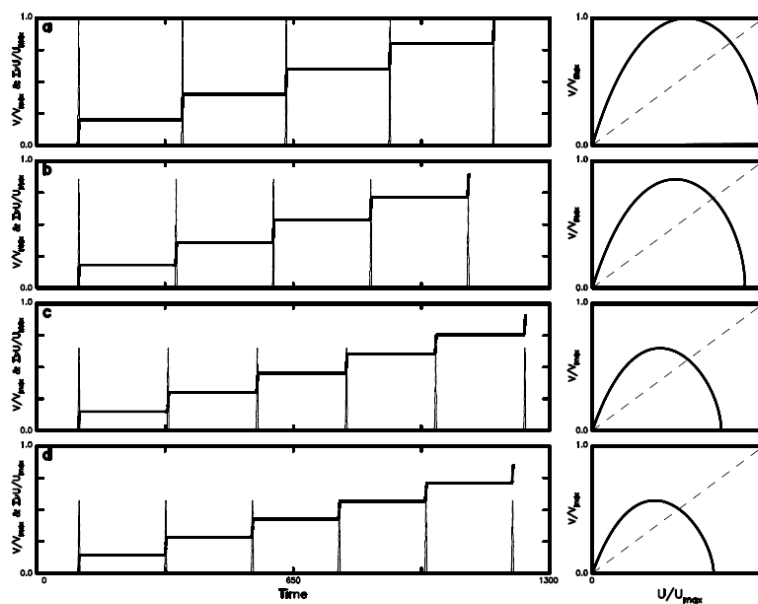
Figure 4. The time variations in V/V_{max} (thin solid line) and cumulative slip $\Sigma U/U_{max}$ (solid line) and the phase portrait of V/V_{max} versus U/U_{max} (solid line) for four values of U_c : (a) for $U_c=0.2$; (b) for $U_c=0.4$; (c) for $U_c=0.8$; and (d) for $U_c=1.0$ when $\eta=0.0$.



736

737

738



739

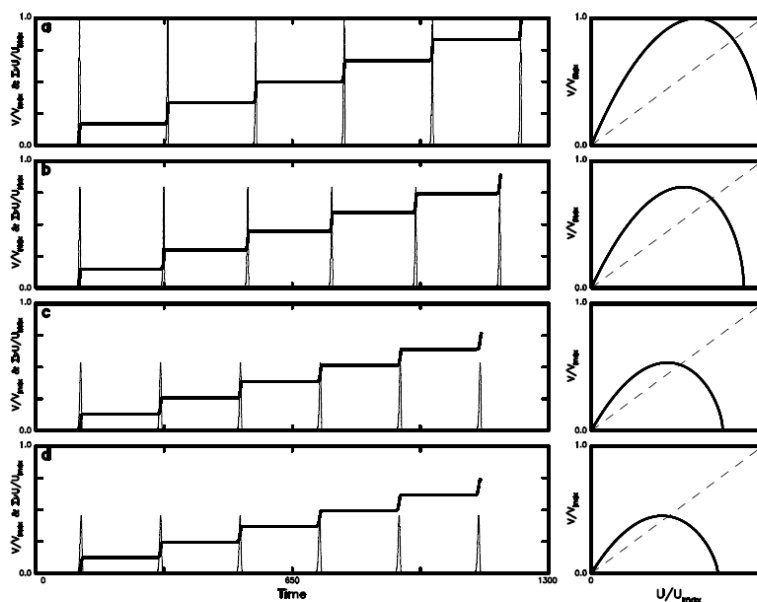
740 Figure 5. The time variations in V/V_{max} (thin solid line) and cumulative slip $\Sigma U/U_{max}$
741 (solid line) and the phase portrait of V/V_{max} versus U/U_{max} (solid line) for four
742 values of η : (a) for $\eta=0.2$; (b) for $\eta=0.4$; (c) for $\eta=0.8$; and (d) for $\eta=1.0$ when
743 $U_c=0.2$.

744

745



746
 747
 748



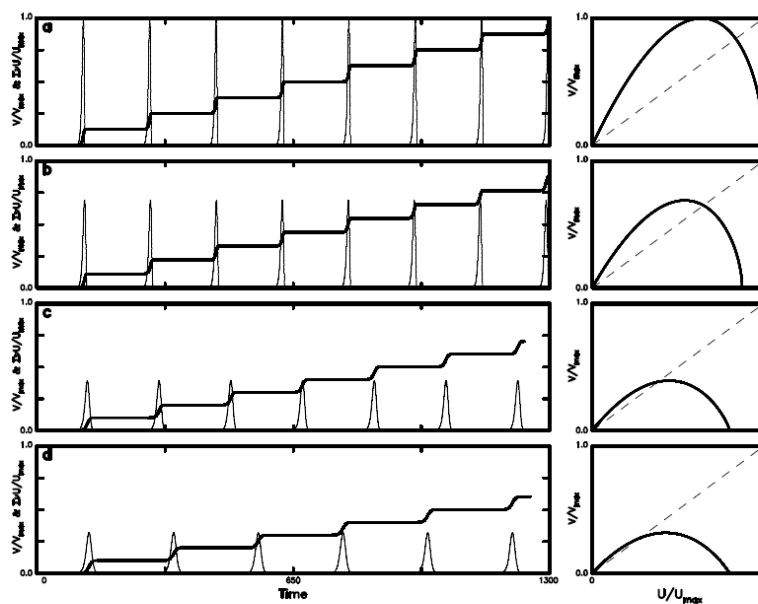
749
 750 Figure 6. The time variations in V/V_{max} (thin solid line) and cumulative slip $\Sigma U/U_{max}$
 751 (solid line) and the phase portrait of V/V_{max} versus U/U_{max} (solid line) for four
 752 values of η : (a) for $\eta=0.2$; (b) for $\eta=0.4$; (c) for $\eta=0.8$; and (d) for $\eta=1.0$ when
 753 $U_c=0.5$.
 754



755

756

757



758

759

760

761

762

763

764

765

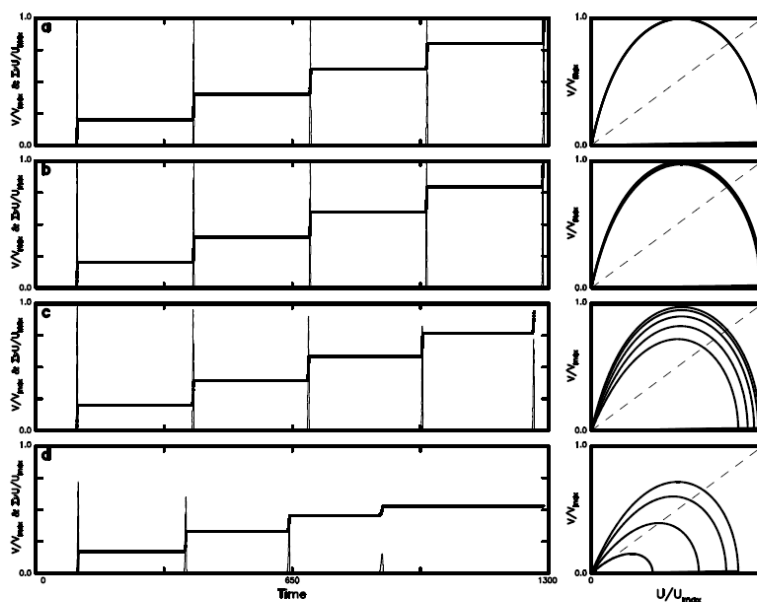
Figure 7. The time variations in V/V_{max} (thin solid line) and cumulative slip $\Sigma U/U_{max}$ (solid line) and the phase portrait of V/V_{max} versus U/U_{max} (solid line) for four values of η : (a) for $\eta=0.2$; (b) for $\eta=0.4$; (c) for $\eta=0.8$; and (d) for $\eta=1.0$ when $U_c=0.8$.



766

767

768



769

770

771

772

773

774

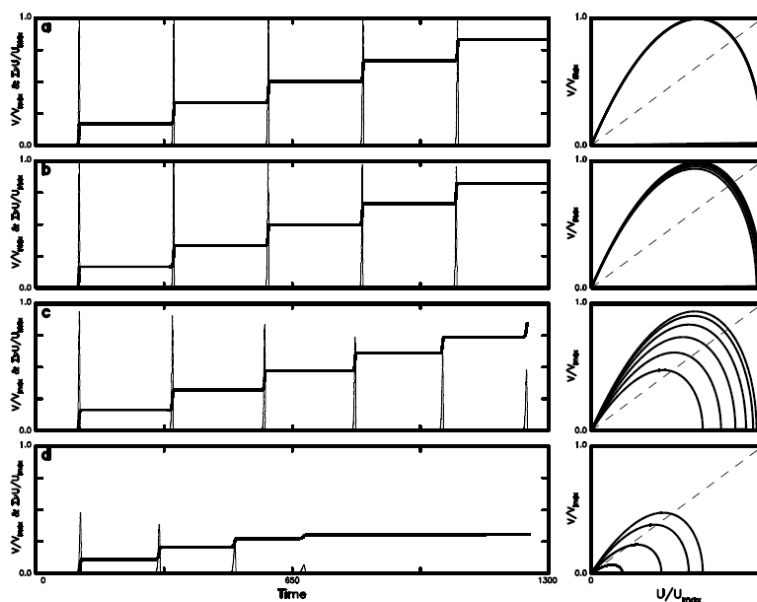
Figure 8. The time variations in V/V_{max} (thin solid line) and cumulative slip $\Sigma U/U_{max}$ (solid line) and the phase portrait of V/V_{max} versus U/U_{max} (solid line) for four values of C : (a) for $C=0.0001$; (b) for $C=0.001$; (c) for $C=0.01$; and (d) for $C=0.05$ when $U_c=0.1$ and $\eta=0$.



775

776

777



778

779

780

781

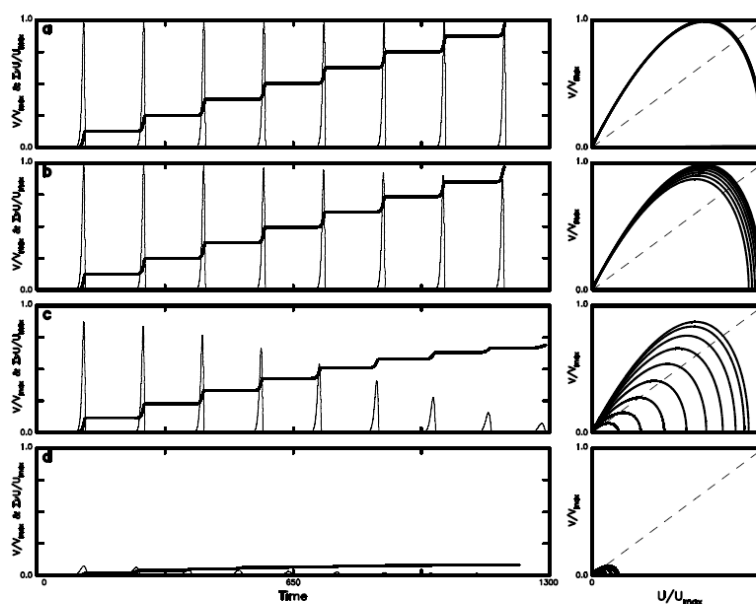
782

783

Figure 9. The time variations in V/V_{max} (thin solid line) and cumulative slip $\Sigma U/U_{max}$ (solid line) and the phase portrait of V/V_{max} versus U/U_{max} (solid line) for four values of C : (a) for $C=0.0001$; (b) for $C=0.001$; (c) for $C=0.01$; and (d) for $C=0.05$ when $U_c=0.5$ and $\eta=0$.



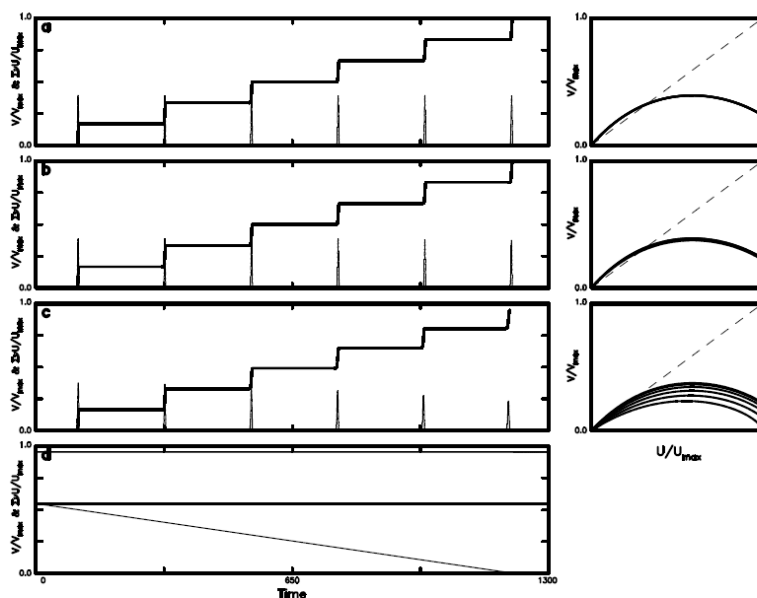
784
785
786



787
788 Figure 10. The time variations in V/V_{max} (thin solid line) and cumulative slip $\Sigma U/U_{max}$
789 (solid line) and the phase portrait of V/V_{max} versus U/U_{max} (solid line) for four
790 values of C : (a) for $C=0.0001$; (b) for $C=0.001$; (c) for $C=0.01$; and (d) for
791 $C=0.05$ when $U_c=0.9$ and $\eta=0$.
792



793
 794
 795

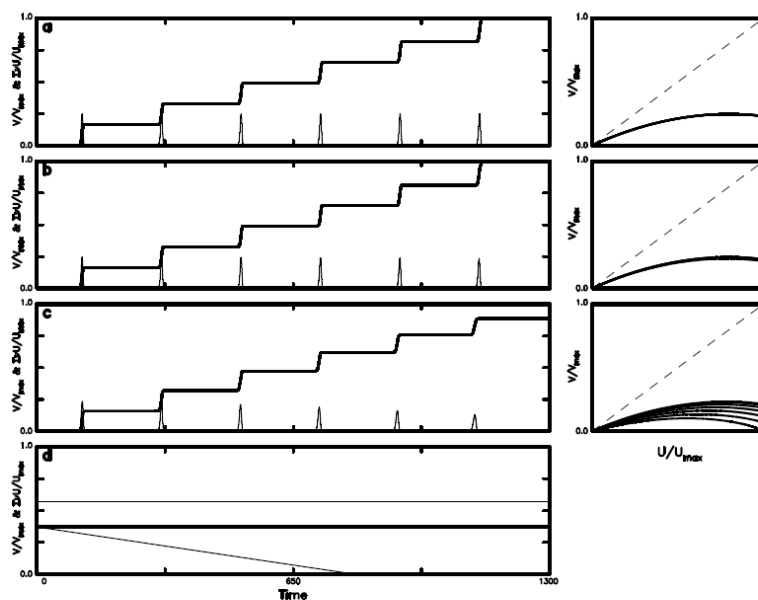


796
 797
 798
 799
 800
 801

Figure 11. The time variations in V/V_{max} (thin solid line) and cumulative slip $\Sigma U/U_{max}$ (solid line) and the phase portrait of V/V_{max} versus U/U_{max} (solid line) for four values of C : (a) for $C=0.0001$; (b) for $C=0.001$; (c) for $C=0.01$; and (d) for $C=0.05$ when $U_c=0.1$ and $\eta=1$.



802
803
804
805



806
807 Figure 12. The time variations in V/V_{max} (thin solid line) and cumulative slip $\Sigma U/U_{max}$
808 (solid line) and the phase portrait of V/V_{max} versus U/U_{max} (solid line) for four
809 values of C : (a) for $C=0.0001$; (b) for $C=0.001$; (c) for $C=0.01$; and (d) for
810 $C=0.05$ when $U_c=0.5$ and $\eta=1$.
811
812